Engineering Failure Analysis 174 (2025) 109482

Contents lists available at ScienceDirect

Engineering Failure Analysis

journal homepage: www.elsevier.com/locate/engfailanal

Investigating hunting stability failure in a high-speed locomotive: A comparative analysis of evaluation methods for typical worn wheel treads

Hu Li [a,b], Tong Tan [b], Sebastian Stichel [c], Yuan Yao [a,*]

[a] State Key Laboratory of Rail Transit Vehicle System, Southwest Jiaotong University, Chengdu, People's Republic of China
[b] Bogie R&D Department, CRRC Zhuzhou Electric Locomotive Co., Ltd., Zhuzhou, People's Republic of China
[c] KTH Royal Institute of Technology, Department of Engineering Mechanics, Stockholm, Sweden

A R T I C L E   I N F O

Keywords:
High-speed locomotive
Three-axle bogie
Hunting stability failure
Equivalent conicity function
Critical speed
Driving energy loss ratio

A B S T R A C T

Hunting stability is a critical factor affecting high-speed locomotives dynamic performance, inherently connected to wheel-rail contact geometry. Tread wear typically increases the non-linearities in the contact geometry, causing stability disparities. Previous studies on stability have often overlooked these nonlinear aspects, which can be captured by the equivalent conicity function. In this study, the equivalent conicity functions of worn wheel treads are systematically categorized into six distinct classes. This classification allows for a comprehensive evaluation of their respective influence on hunting stability failure, enabling the analysis of stability characteristics of typical worn wheel treads. The limited research available on three-axle bogies motivate the selection of a locomotive equipped with such bogies as the basis for framework, aiming to bridge the gap in existing literature. Based on different stability evaluation methods, theoretical, small-amplitude hunting, and engineering critical speeds have been determined. The observed differences in different critical speeds from the perspective of equivalent conicity function are elucidated. The results show that a high equivalent conicity at small displacement can significantly reduce the theoretical critical speed, and therefore, the engineering critical speed is recommended as a criterion for stability assessment and optimization. Moreover, the Driving Energy Loss Ratio (DELR), a metric assessing both primary and secondary hunting stability, is developed to evaluate the stability of self-excited vibrations. This research provides guidance for the evaluation and optimization of railway vehicle stability.

1. Introduction

The stability of the hunting motion determines the critical speed of trains. When hunting stability failure occurs, the ride comfort will be deteriorated and the safety of the train can be affected, potentially leading to derailment and track damage. Hunting stability is mainly related to vehicle suspension parameters and wheel-rail contact geometry. Reasonable suspension parameters and wheel-rail contact geometry matching can ensure that the critical speed is higher than the operational speed of the vehicle. Suspension parameters are typically more or less constant during operation, the geometry of wheel-rail contact, however, is dynamic and prone to change as a result of wear on both the wheel and rail. The stability of trains is very sensitive to the change in the wheel-rail contact

* Corresponding author.
E-mail address: yyuan8848@163.com (Y. Yao).

https://doi.org/10.1016/j.engfailanal.2025.109482
Received 13 January 2025; Received in revised form 9 February 2025; Accepted 3 March 2025
Available online 4 March 2025
1350-6307/

geometry at high speed, so the stability problems caused by wheel-rail wear should be paid attention to.

Field measurements have shown that the equivalent conicity changes with wheel-rail wear and the change of conicity effects stability [1–8]. Wheel-rail wear prediction is an important means to guide the wheel-rail maintenance schedules. The common wheel-rail wear prediction strategy nowadays relies on an iteration of dynamic simulations with co-simulation techniques [9–14]. Several scholars have proposed rapid wear prediction methods to reduce the often long computation times [15–18]. Data driven prediction of wheel-rail wear has been a hot topic in recent years. A two-step data-driven wear prediction method that can predict the overall wear trend of the train has been presented recently [19]. The application of active suspension and the optimization of wheel-rail profile matching have proven to be an effective method to delay the formation of sever tread wear and improve stability [20–25]. The above research reduces the harm caused by wheel-rail wear with help of field measurements, wear prediction, active suspension and profile optimization. However, wheel-rail wear is inevitable, and the impact of wheel-rail wear on stability failure should be studied.

The influence of wheel-rail wear on stability is due to the change of wheel-rail contact geometry. Therefore, this paper studies the influence of wheel-rail contact geometry on stability. The common parameter used to evaluate the geometric characteristics of wheel-rail contact is equivalent conicity, and the International Union of Railways defines the equivalent conicity corresponding to a hunting movement amplitude of 3 mm as the nominal equivalent conicity [26]. The nominal equivalent conicity is widely used to characterize worn wheels, however, it is only suitable for slightly worn wheel treads. With the intensification of wheel-rail wear, the geometric characteristics of wheel-rail contact will show more and more nonlinearity. Polach proposed a nonlinear parameter as a supplement to the nominal equivalent conicity to consider the nonlinear wheel-rail contact geometry [27,28]. On the basic of nonlinear parameters, many scholars have made further research [29–31]. Previous studies on the stability have primarily focused on Bo-Bo vehicles equipped with two-axle bogies, with scant research dedicated to Co-Co locomotives featuring three-axle bogies [32,33], particularly in the context of high-speed locomotives. Locomotive are characterised by high axle load and large traction power, so the wheel-rail wear is more serious, and the nonlinear degree of wheel-rail contact geometry is also higher. In the research and development of high-speed locomotive, the nonlinear wheel-rail contact needs to be studied more deeply. In this study, different worn treads are classified from equivalent conicity functions to study their influence on locomotive stability.

The layout of this paper is as follows. In Section 2, the locomotive dynamics model is established. Section 3 introduces the tread inversion method based on a Worn Tread Database, and the corresponding worn tread of different equivalent conicity functions is obtained. In Section 4, different stability evaluation methods are introduced, and the indictor of Driving Energy Loss Ratio (DELR) is proposed. In Section 5, the stability characteristics of a locomotive corresponding to different equivalent conicity functions is analyzed by different stability evaluation methods. Section 6 concludes this paper.

2. Modeling and validation

This section introduces the establishment process of the locomotive dynamic model and validation of the accuracy of the model by comparison with measurements.

2.1. Locomotive dynamics model

The traction equipment of the investigated EMU (electric multiple units) is concentrated on the locomotive at both ends of the train, and the structure of the locomotive is more complex than that of the power car of the EMU with distributed power. Based on actual dynamic parameters of a locomotive operating in China, a rigid multi-body dynamics model of the locomotive is established in the

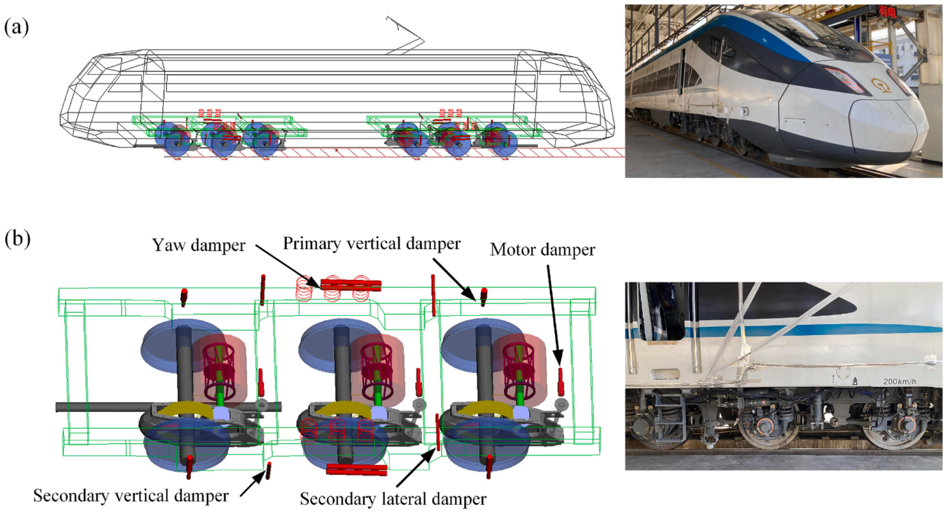

Fig. 1. Locomotive dynamics model: (a) locomotive model; (b) bogie model.

multi-body dynamics simulation software SIMPACK. As shown in Fig. 1, the dynamics model, with 124 degrees of freedom, consists of 47 rigid bodies, including one carbody, two bogie frames, two traction rods, six wheelsets, six motors, six rotors of the motors, six gearboxes, six drive gears, six passive gears and six gearbox steeves. The primary suspension of the locomotive acts between the wheelset and the bogie frame, comprising the axle box springs and the primary vertical dampers. The secondary suspension operates between the bogie frame and the carbody, including lateral dampers, yaw dampers, vertical dampers, air springs and anti-roll bars. The motor mount is connected to the frame via bushings, motor bump stops and motor dampers. The dampers shown in Fig. 1(b) are represented by a piecewise linear Maxwell damper model. The nonlinear characteristics of dampers and secondary bump stop are considered. The wheel-rail creep force is calculated by the FASTSIM algorithm [34].

The main parameters of the locomotive are shown in Table 1.

2.2. Model validation

To validate the accuracy of the dynamic model, on-board testing was conducted on the locomotive operating on the Chengdu-Kunming Railway, with the results compared against outcomes from dynamic simulations. In the dynamic simulation, the wheel-rail profile was set to JM3 standard wheel profiles and measured rail profiles to keep consistent with the test conditions. The JM3 wheel profile, a wear-type design, is specifically tailored for locomotives operating on large-radius curves and straight tracks in China. The testing involved measuring the acceleration of carbody and the calculation of ride indexes, which were then compared with the results of the dynamic simulation. This validation approach, widely adopted in numerous studies[2,35,36], has proven to be effective.

Acceleration sensors were installed beneath the driver's seat, as depicted in Fig. 2(a). The collected acceleration time series were segmented into 5-second intervals to calculate the ride index. Fig. 2(b) displays the comparison between simulation and measurement results, and the operating speed is 200 km/h. Upon comparing the maximum values of lateral acceleration, it is observed that the simulation and measurement results are closely aligned, both peaking at approximately 0.8 m/s^2. The comparison of ride index indicates that while the simulation results exhibit a slightly narrower range of variation, both the simulated and measured values center around 2.2. Fig. 2(b) and (c) present the Short-Time Fourier Transform (STFT) spectrum of lateral acceleration for both simulation and measurement. It is evident that the principal frequency of the carbody's lateral acceleration is nearly 1.1 Hz in both cases. The results derived from the simulation are fundamentally consistent with the measurements, thereby confirming the accuracy and rationality of the dynamic model.

3. Tread inversion for targeted conicity

3.1. Equivalent conicity

Owing to factors such as wheel-rail wear, changes in rail cants, and deviations of gauge width, the geometry of wheel-rail contact can exhibit variability [37], which poses challenges to running stability. Consequently, there is a necessity to employ a simple yet rational parameter to characterize the wheel-rail contact geometry. Polach has highlighted that the sensitivity of running stability to the equivalent conicity is high and the conicity is the only parameter usually mentioned in connection with the wheel/rail contact geometry [27].

The essence of equivalent conicity is a function of the difference in rolling radius and the lateral displacement of the wheelset. The nominal equivalent conicity defined by the International Union of Railways (UIC) refers to the equivalent conicity at a lateral displacement of 3 mm, which is a commonly used indicator for linearizing wheel-rail contact [26]. The equivalent conicity function of the majority of standard wheel and rail profiles does not vary significantly with the lateral displacement of the wheelset as long as the contact point is on the wheel tread, allowing the nominal equivalent conicity to adequately assess the relationship between wheel-rail contact geometry. However, tread wear introduces considerable nonlinearity in the wheel-rail contact, rendering the nominal equivalent conicity inadequate for capturing this complexity. The methods that are frequently used to calculate the equivalent conicity are harmonic linearization, equivalent linearization by the application of Klingel formula used by UIC and linear regression of the rolling radii difference function [27]. In SIMPACK, the equivalent conicity is primarily calculated using the harmonic linearization and quasi-elastic methods.

Table 1
Main dynamics parameters.

Name	Value	Unit
Length between bogie centers	10.07	m
Front bogie wheel base	1.8 + 2	m
Rear bogie wheel base	2 + 1.8	m
Wheel rolling radius	0.525	m
Lateral wheel distance	0.7465	m
Axle load	17	t
Bogie mass	21	t
Carbody mass	60	t
Operation speed	200	km/h
Track gauge	1.435	m

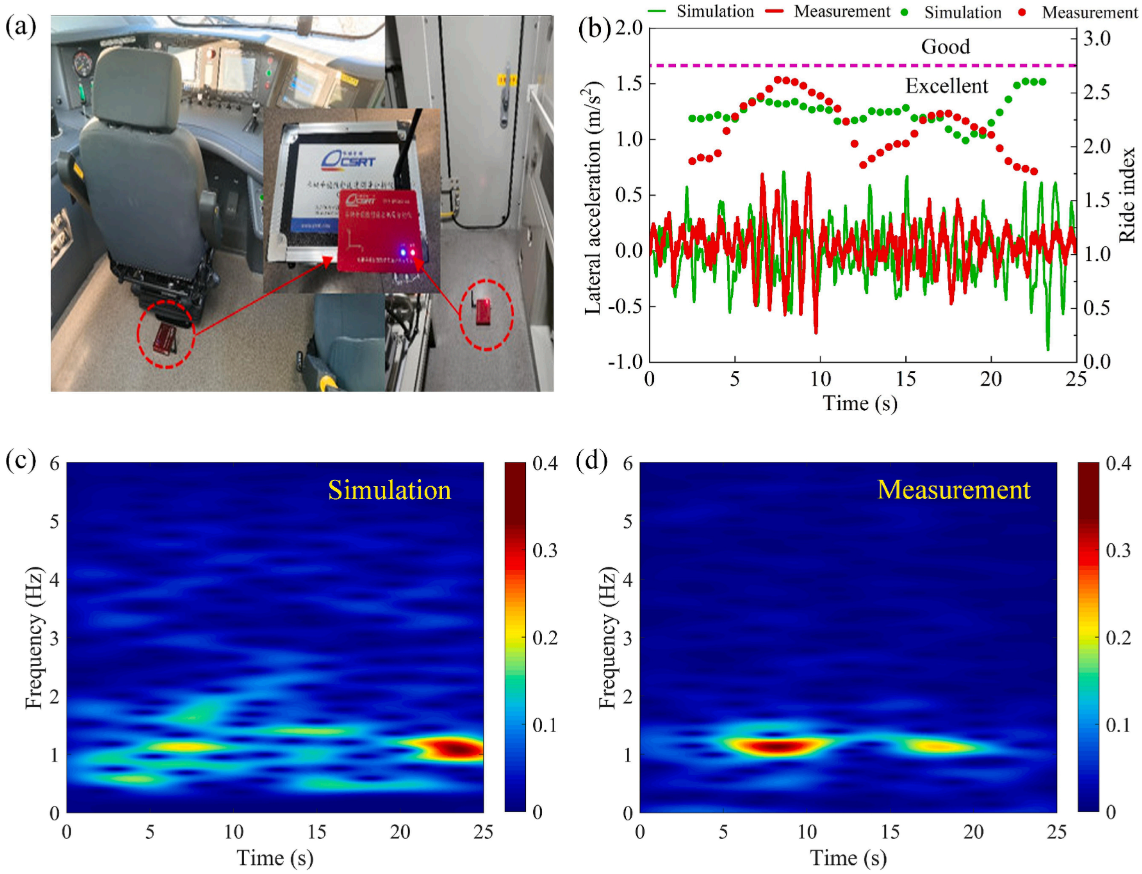

Fig. 2. Comparison of dynamic performance between measurement and simulation: (a) Installation position of the acceleration sensor; (b) Lateral acceleration and ride index; (c) STFT spectrum of lateral acceleration from simulation; (d) STFT spectrum of lateral acceleration from measurement.

3.2. Worn Tread Database

The Worn Tread Database is a repository that encompasses tread measurements. Through systematic organization of data from measurements, an extensive dataset comprising 128 distinct worn wheel profiles was compiled. The study focuses on the equivalent conicity function, assuming identical profiles for the left and right wheels to reduce unnecessary computational complexity. Because rail wear is slow and regularly maintained, a default rail profile of CN60 with a rail cant of 1/40 is assumed. As shown in Fig. 3, the equivalent conicity function for each wheel profile has been determined using the method of harmonic linearization and quasi-elastic correction, which are widely utilized within SIMPACK. From Fig. 3(b), it is observed that there is a sudden increase in equivalent conicity when the lateral displacement exceeds 7 mm. This is attributed to the fact that when the lateral displacement is too large, the

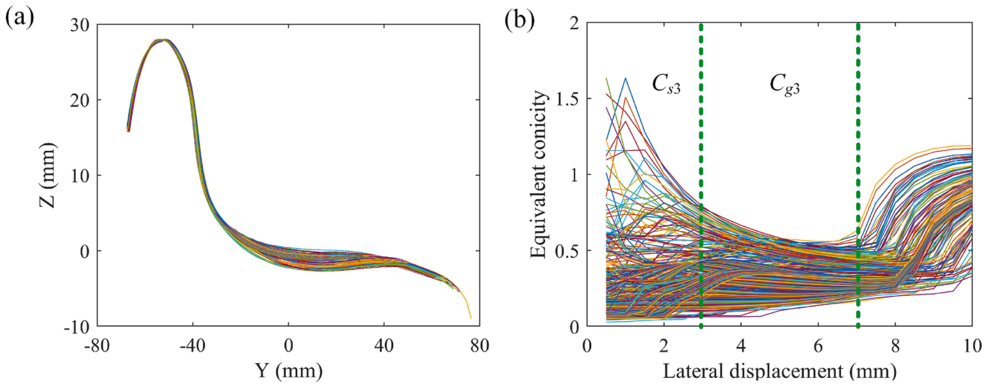

Fig. 3. Worn Tread Database results: (a) wheel profiles; (b) functions of equivalent conicity.

wheel-rail contact point approaches the flange, leading to flange contact. At this point, the difference in the diameters of the left and right wheels increases significantly, thereby causing an increase in equivalent conicity. However, this occurrence is primarily associated with negotiation of tight curves and has negligible influence on the stability of vehicles on straight track. Consequently, this scenario lies outside the parameters of the current study. The term C_3 is defined as the equivalent conicity at a lateral displacement of precisely 3 mm. As seen in Fig. 3b, C_{s3} represents the equivalent conicity for displacements less than 3 mm, and C_{g3} refers to the equivalent conicity for displacements between 3 mm and 7 mm.

Fig. 3(b) clearly illustrates that the range of variation for C_{s3} is broader than that for C_{g3}. Therefore, C_{s3} is divided into three clear categories, labeled as H for High, M for Medium, and L for Low. Similarly, C_{g3} values are divided into two groups, indicated by H for High and L for Low. To enhance the clarity and readability, the classifications of HL and HH have been unified under the single designation HX. Likewise, HH, MH, and LH types have been collectively termed XH. The X here does not represent a specific classification, but is used to indicate a unified approach. The same method has been applied to LX and XL. This stratification of the equivalent conicity functions yields six distinct combinatorial patterns, as detailed in Table 2, providing a comprehensive framework for analysis.

Table 2 illustrates a notable disparity in the distribution of the six combinations within the Worn Tread Database, where the LH combination accounts for the largest share, followed by the HH combination with the smallest one. It should be noted that this study selects C_3 as a reference value due to its alignment with the nominal equivalent conicity value. However, the designation of C_3 as a reference is not the only option.

3.3. Worn tread inversion process

When examining the impact of the equivalent conicity function on vehicle stability, the method of control variates offers an effective research tool. This approach allows us to precisely identify the specific effects of changes in the equivalent conicity function on vehicle stability. Therefore, for the six equivalent conicity functions described in Table 2, we aim to select six typical worn wheel tread profiles with the following criteria:

1. HH and HL should exhibit similar values of C_{s3}, MH and ML should exhibit similar values of C_{s3}, and LH and LL should exhibit similar values of C_{s3}.
2. HH, MH, and LH should exhibit similar values of C_{g3}, while HL, ML, and LL should exhibit similar values of C_{g3}.
3. The nominal equivalent conicity of the six wheel tread profiles should be similar.

These criteria facilitate the study of the impact of C_{g3} and C_{s3} on vehicle stability. However, the equivalent conicity functions of measured worn tread profiles show significant dispersion, making it challenging to meet these criteria directly. To address this challenge, we propose a method to optimize the profiles of worn treads. It is crucial to clarify that this optimization does not aim to enhance dynamic performance through profile modification. Instead, the objective is to refine the worn wheel profiles to better satisfy the three fundamental criteria established in the preceding analysis. Through optimization, we aim to obtain a set of typical worn wheel tread profiles that meet the aforementioned criteria, thereby providing a reliable experimental foundation for further stability research.

The optimization of worn tread profiles can be regarded as the worn tread inversion, and the general architecture of the worn tread inversion process is shown in Fig. 4.

Firstly, the target equivalent conicity function is established, representing a set of equivalent conicities corresponding to specific displacements. The selection of these specific displacements is guided by the principle of effectively characterizing the features of the equivalent conicity function. Typically, we select five displacements: 0.5 mm, 1 mm, 3 mm, 4 mm, and 6 mm. Subsequently, the Mean Squared Error (MSE) of each equivalent conicity function within the Worn Tread Database is calculated with respect to the target function, as delineated in the subsequent formula:

$$\mathrm{MSE}(i) = \sqrt{\sum_{k=1}^{n} \frac{\left(C_{obj}(k) - CT_i(k)\right)^2}{n}} \tag{1}$$

where n represents the number of the specific displacements, C_{obj} denotes the target equivalent conicity function, and CT_i represents the equivalent conicity function of the i-th tread within the Worn Tread Database.

Table 2
Six combinatorial schemes for equivalent conicity functions.

C_{s3_mean} vs C_3	C_{g3_mean} vs C_3	Combination	Percentage
$C_{s3\_mean} > 1.05C_3$	$C_{g3\_mean} \geq C_3$	HH	6.97 %
$C_{s3\_mean} > 1.05C_3$	$C_{g3\_mean} < C_3$	HL	12.2 %
$0.95C_3 \leq C_{s3\_mean} \geq 1.05C_3$	$C_{g3\_mean} \geq C_3$	MH	9.45 %
$0.95C_3 \leq C_{s3\_mean} \geq 1.05C_3$	$C_{g3\_mean} < C_3$	ML	8.21 %
$C_{s3\_mean} < 0.95C_3$	$C_{g3\_mean} \geq C_3$	LH	43.3 %
$C_{s3\_mean} < 0.95C_3$	$C_{g3\_mean} < C_3$	LL	19.9 %

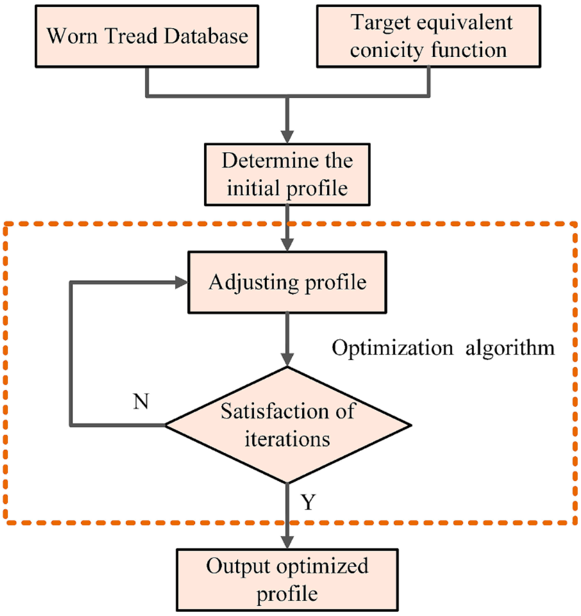

Fig. 4. General architecture of the worn tread inversion process.

The process begins with the selection of the tread profile associated with the equivalent conicity function that exhibits the minimum MSE as the initial profile. The region of the tread that maintains consistent contact with the rail is then identified as the zone for adjustment. Within this zone, six points are equidistantly selected and designated as design variables, as depicted in Fig. 5. The vertical coordinates of these points are subsequently modified, and a cubic spline is employed to generate a new curve, which replaces the adjusted segment, resulting in an optimized tread profile. A particle swarm optimization algorithm based on adaptive grid algorithms is utilized to determine the tread profile that closely aligns with the target equivalent conicity function.

A nominal equivalent conicity of 0.4 is specified, and six categories of equivalent conicity functions are selected from Table 2 to serve as target function. The worn tread inversion method has been utilized to obtain the profiles of worn treads, and their equivalent conicity functions have been calculated, as illustrated in Fig. 6.

4. Evaluation method of the lateral stability

The lateral stability of locomotives is a crucial measure for evaluating operational safety. However, the various approaches available for assessing this stability can result in a variety of outcomes [38]. This subsection begins by explaining the methodologies for evaluating locomotive lateral stability as prescribed by European and Chinese standards, highlighting their suitability for real-time monitoring during operation and acknowledging their susceptibility to variations in track conditions. The discussion then shifts to

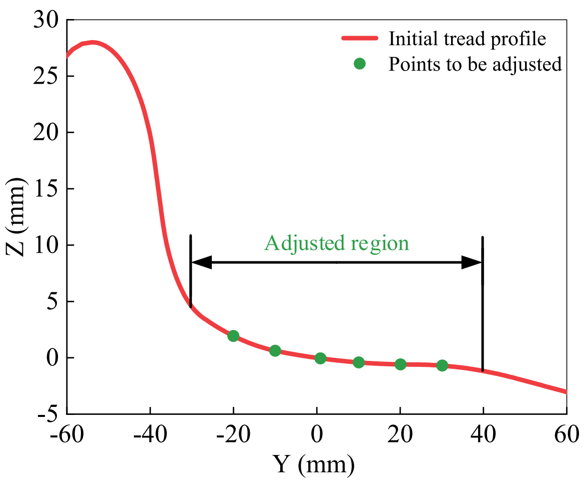

Fig. 5. Illustration of design variables.

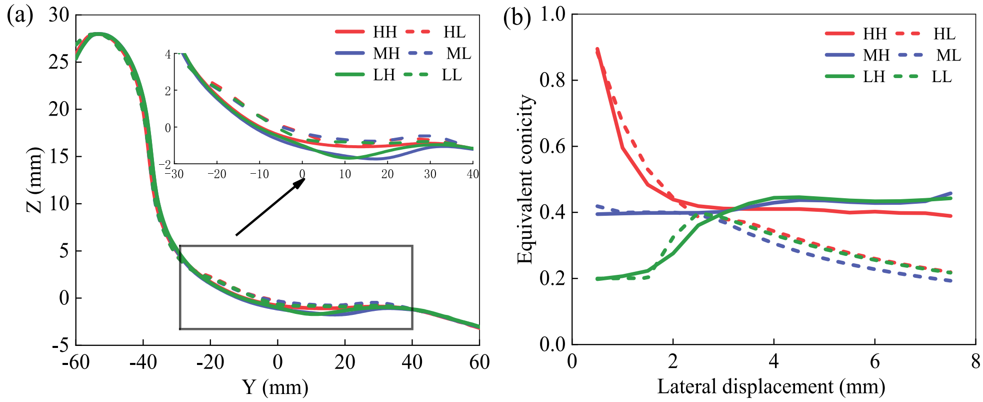

Fig. 6. Worn tread inversion results: (a) wheel profiles; (b) functions of equivalent conicity.

methodologies rooted in systemic stability theory for resolving hunting stability. Concluding the section, an innovative metric termed the DELR is introduced from the vantage point of energy dissipation inherent in hunting motion, tailored for the assessment of lateral stability within dynamic simulation environments.

4.1. *Standard method*

4.1.1. *EN14363-based method*

In accordance with the standards outlined in EN14363 [39], the critical speed is assessed by analyzing the lateral acceleration of the bogie frame or the lateral axle box force during the operation of the vehicle on a track with given track irregularities. The data processing for the lateral acceleration of the bogie frame and the lateral axle box force incorporates a band-pass filter with a passband of $f_0 \pm 2$ Hz, where f_0 denotes the dominant frequency in case of unstable running behavior. Additionally, a sliding root mean square (RMS) method is applied, featuring a window length of 100 m and a step length that does not exceed 10 m. Then, the extracted maxima are compared against the limit value in the standard to determine if the vehicle behaviour is unstable.

The limit value of the lateral acceleration of the bogie frame is defined as:

$$A_{\text{lim}} = \frac{1}{2}\left(12 - \frac{m_b}{5}\right) \tag{2}$$

with A_{lim} expressed in m/s^2 and m_b being the mass of the bogie in tons.

For the lateral axle box forces, the limit value is defined as 50 % of the Prud's Homme limit:

$$\sum Y_{\text{lim}} = \frac{1}{2}\left(10 + \frac{P_0}{3}\right) \tag{3}$$

with P_0 the axle load and both P_0 and Y_{lim} defined in kN.

4.1.2. *GB/T5599-based method*

According to the provisions of GB/T5599-2019[40], the bogie frame position directly above the axle box is designated as the measurement point for bogie frame acceleration. The lateral acceleration data, once measured, is band-pass filtered with a specified passband of 0.5–10 Hz. The vehicle is considered unstable if a sequence of six consecutive peak lateral accelerations surpasses a threshold of 8 m/s^2. However, the standard does not provide a metric for evaluating stability performance; the results are simply classified as stable or unstable. To demonstrate how stability changes, a novel metric, denoted as $AP(t)$, is introduced. This metric represents the minimum value among the six consecutive peak accelerations centered around a specific time point t within the time domain data. Therefore, the vehicle is deemed to be unstable when the maximum value of $AP(t)$ exceeds 8 m/s^2.

When assessing stability based on bogie acceleration, there is a distinct difference in data processing between European and Chinese standards. The European standard prioritizes the RMS value across the frequency range associated with instability, whereas the Chinese standard concentrates on the extreme values within the 0.5–10 Hz frequency band. Interestingly, the threshold set by the European standard rises with a decrease in bogie mass, while the Chinese standard maintains a constant threshold of 8 m/s^2. As a result, for bogies with lower mass, the critical speed derived from the European standard is likely to exceed that of the Chinese standard. In contrast, for bogies with higher mass, the situation is reversed.

4.2. *Hunting stability*

The acceleration of the bogie frame serves as readily measurable parameter for assessing vehicle stability during operation. Nonetheless, from the point of vehicle system dynamics, the vehicle stability is ascertained by the presence of hunting motion, which is a unique phenomenon to railway vehicles. This motion enables the wheelset to realign with the track center when subjected to geometric irregularities along the tangential direction of the track. However, an increase in velocity may cause the wheelset to vibrate violently and potentially result in hunting instability [41]. The stability of the hunting motion is typically evaluated through three methods: the root loci method for linear stability analysis, and the constant speed method and the decreasing speed method for the evaluation of nonlinear stability.

a) Root loci method: The root loci method involves analyzing the relationship between the eigenvalues of the Jacobian matrix and the parameters of the vehicle system. Instability in the system is indicated when the real part of the eigenvalues associated with the hunting motion mode crosses the imaginary axis.
b) Constant speed method: The constant speed method entails the vehicle system traversing a track section with irregularities at a constant speed, followed by operation on a smooth track segment. This approach involves scrutinizing the convergence of the limit cycle of the wheelset lateral displacement to judge wether the system is stable[42,43]. Due to the discrete nature of velocity increments, a large volume of simulations is required to ensure the precision of the solution. To augment computational efficiency, workstations or servers with parallel computing capabilities are typically utilized.
c) Decreasing speed method: The vehicle is forced into hunting instability at high speed upon encountering a short segment of irregular track. Subsequently, the operating speed is reduced while traveling on a smooth track. The critical speed is reached when a stable motion of the vehicle is achieved [38,44].

The hunting motion can be disrupted in some cases if a track geometry irregularity is sufficiently large and suitably positioned to disrupt the cyclic motion [41]. In both the constant and decreasing speed methods, the spatial wavelength of track irregularities employed to induce hunting motion should be carefully calibrated to enhance the likelihood of inciting such motion.

4.3. Driving energy Loss Ratio (DELR)

The hunting motion is a type of self-excited vibration, wherein the input energy is sourced from kinetic energy and driving forces. This input energy increases as the stability of the hunting motion diminishes. Consequently, the decline in stability leads to an increase in input energy, which in turn, aggravates the system's instability. To address this, we propose an evaluation of stability from the perspective of energy dissipation. We develope an indicator known as the Driving Energy Loss Ratio (DELR), which serves to assess the stability by quantifying the energy dissipated during the hunting motion.

The DELR represents the power of kinetic energy dissipation per unit mass, denoted as P (unit: W/kg), as shown in the following equation:

$$P \equiv \frac{\Delta E}{mt} \tag{4}$$

where ΔE represents the amount of kinetic energy dissipated, with m and t corresponding to the mass of the vehicle and the operation time, respectively. The dissipation of kinetic energy, ΔE, is given by:

$$\Delta E = \frac{m(v_t^2 - v_0^2)}{2} \tag{5}$$

where v_t and v_0 represent the velocity at time t and the initial velocity, respectively. By substituting Eq. (5) into Eq.n (4), we derive the general expression of P:

$$P = \frac{v_t^2 - v_0^2}{2t} \tag{6}$$

Because the presence of track irregularities can cause fluctuations in speed, we do not evaluate stability at each time step in the practical application of DELR. Our approach is to let the vehicle pass through a section of rough track, which is set to be 800 m long, and then run on a smooth track. We use the predetermined initial speed v_0 and the final speed v_t on the smooth track, substituting these values into Eq. (6) for calculation. It is evident that this treatment is consistent with that in the constant speed method, where the vehicle is required to pass through a section of rough track and then run on a smooth track.

5. Numerical investigations

This section employs the inversely derived wear profile as computational input and applies various stability assessment methods to determine the lateral stability and critical speeds of high-speed locomotives. From the standpoint of stability theory, the existence of a limit cycle is a sign of inherent system instability. However, a limit cycle with a minor amplitude does not lead the locomotive to surpass the threshold values set forth in vehicle acceptance specifications, such as those in the EN14363 and GB/T5599-2019 standards. To more accurately characterize the critical speed, this study adopts the following definitions:

- The theoretical critical speed is defined as the speed at which the limit cycle vanishes. The decreasing speed method is subject to velocity inertia, which can affect the accuracy of the theoretical critical speed. Therefore, the constant speed method is employed to determine the theoretical critical speed.
- The small-amplitude hunting critical speed corresponds to the first drop of the limit cycle in amplitude when employing the decreasing speed method [38]. Below this speed threshold, small-amplitude hunting may exist, but big-amplitude hunting is not observed.
- The engineering critical speed is defined by the acceptance criteria or standards, as detailed in Section 4.1.

5.1. Hunting stability analysis

The decreasing speed method effectively reveals the relationship between hunting movement and velocity reduction, serving as an excellent approach for analyzing the hunting stability. The locomotive's velocity was initialized at 700 km/h, with a deceleration rate set to 5.56 m/s2. A track irregularity spectrum with a duration of 2 s was then introduced to the vehicle system. The structure of the track irregularities was described by their power spectral density, with spatial wavelengths ranging from 40 to 100 m and a frequency count set at 30. This configuration aims to approximate the disturbance frequencies experienced by the locomotive at 700 km/h to its hunting motion frequencies, thereby increasing the likelihood of system instability and facilitating the study of such dynamic behaviors. The results obtained by the decreasing speed method are shown in Fig. 7 (a) and (b).

The results depicted in Fig. 7(a) and (b) reveal that an decreased C_{s3} value is associated with a higher theoretical critical speed. However, a lower C_{g3} value does not lead to an increase in the small-amplitude hunting critical speed. To validate the findings, the standard JM3 tread, which is the standard wheel profile for locomotives in China, was included as an additional computational parameter. This is because it has a smaller C_{g3} and C_{s3} compared to worn treads. For the standard JM3 tread, the C_{g3} and C_{s3} values fall within the range of 0.1–0.2, with the detailed contact geometry characteristics reported in reference [45]. As depicted in Fig. 7(c), the results indicate that the small-amplitude hunting and theoretical critical speeds for the standard JM3 tread are in close proximity. Notably, the small-amplitude hunting critical speed of the JM3 tread is lower compared to the other worn treads, while the theoretical

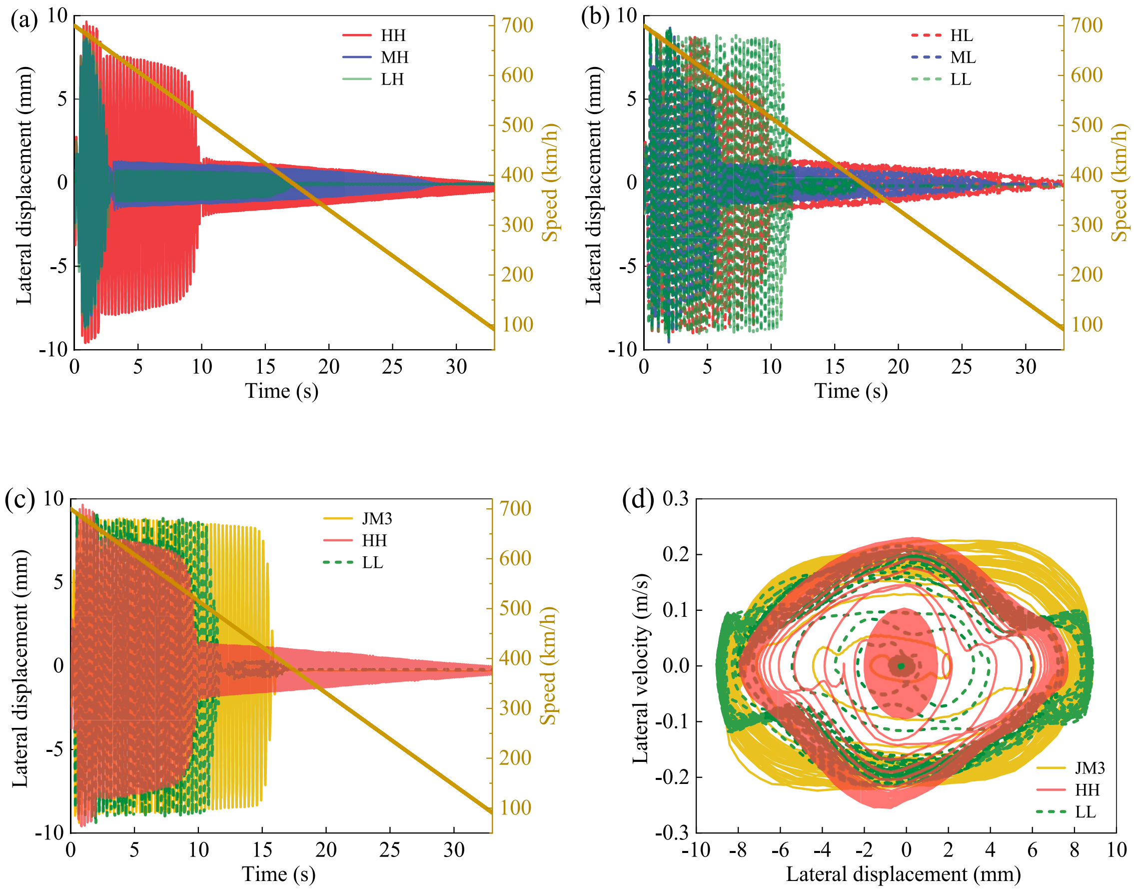

Fig. 7. Decreasing speed method results: (a) amplitude-time profile for XH; (b) amplitude-time profile for XL; (c) amplitude-time profile for JM3, HH, and LL; (d) phase diagram results for JM3, HH, and LL.

critical speed is higher, which supports the conclusions drawn.

Table 3 presents the frequencies of hunting motion for locomotives with various treads during the deceleration stage. Table 3 indicates that within the operating speed range of 400–600 km/h, the frequency of large-amplitude hunting motion is around 3.5 Hz. The frequency of small-amplitude hunting motion is comparatively higher and exhibits a positive correlation with the C_{s3} values.

To elucidate the results depicted in Fig. 7, the model was linearized to obtain the root loci at various speeds as the equivalent conicity changes. During the linearization of the wheel-rail contact, the contact angle and rolling angle were defined as linear functions of conicity, with coefficients of 80 for the contact angle and 0.4 for the flange rolling angle, as cited in [46]. Due to the approximate 0.5 mm lateral clearance in the axle box bearings, the primary lateral stiffness exhibits nonlinearity. The relationship between the lateral force on the axle box F and the lateral displacement of the wheelset relative to the bogie frame Y_{w2b} is illustrated in Fig. 8(a). The formula for calculating the equivalent stiffness Keq is shown in the following equation:

$$Keq = \begin{cases} 0 & Y_{w2b} \leqslant 0.5 \\ \dfrac{K(Y_{w2b} - 0.5)}{Y_{w2b}} & Y_{w2b} > 0.5 \end{cases} \tag{7}$$

where K represents the lateral stiffness of axle box, with a value of 5.1 kN/mm. The equivalent stiffness Keq calculated by Equation (7) is shown in Fig. 8 (b).

Let Y_{w2b} take the values of 0.5 mm, 0.75 mm, 1 mm and 8.5 mm for the linearization of the primary lateral stiffness. The results are shown in Fig. 9.

In Fig. 9, the horizontal axis represents the mode damping ratio ζ, and the vertical axis represents the damped vibration frequency of mode. Each root loci plot consists of 29 eigenvalue sets, corresponding to conicities ranging from 0.1 to 1.5. The 'o' symbols mark the modes, with larger symbols indicating higher conicities. The hunting motion is distinctly highlighted. Theoretically, a system is deemed unstable when its damping ratio falls below zero; however, for a more conservative engineering approach, this study adopts a threshold of 0.05. The figure includes two red dashed lines that signify the theoretical and engineering instability thresholds.

The results in Fig. 9(a) ~ (c) can explain the phenomenon of small-amplitude hunting, while those in Fig. 9(d) can account for large-amplitude hunting. From Fig. 9(a) ~ (c), it can be concluded that when Y_{w2b} is small, smaller values of Y_{w2b} lead to poorer stability, and larger equivalent conicity also results in poorer stability. When the amplitude of hunting is small, Y_{w2b} is also small, leading to poor stability, thus causing an increase in the amplitude of hunting. An increase in the amplitude of hunting leads to an increase in Y_{w2b} and changes in equivalent conicity, thereby keeping the amplitude of hunting within a relatively fixed range.

In Fig. 9(a), at speeds of 400 km/h and 600 km/h, all conicities are unstable. At 200 km/h, the damping ratio ζ begins to be greater than zero when the conicity is less than 0.5. The C_{s3} value for HX is greater than 0.5, so at 200 km/h, HX still exhibits small-amplitude hunting. When Y_{w2b} reaches 0.75 mm, as shown in Fig. 9(b), all conicities are stable at 200 km/h. Therefore, in Fig. 7, when the speed drops to 200 km/h, the amplitude is very small, below 0.75 mm. In Fig. 9(d), when Y_{w2b} is large, stability does not continue to deteriorate with increasing conicity. At 200 km/h, system stability diminishes with increasing equivalent conicity but does not result in instability. Upon elevating the velocity to 400 km/h, stability initially drops and then improves with rising conicity, reaching a critical juncture at 0.3, where it is closest to the engineering threshold without crossing it. Ultimately, at a velocity of 600 km/h, the pattern of stability variation mirrors that at 400 km/h, yet the critical juncture occurs earlier at an equivalent conicity of 0.15, marking the point where system stability deteriorates to its minimum and enters an unstable condition.

5.2. Stability results considering track excitation

The high-speed locomotive in this study operates on the Existing Railway in China, which is characterized by ERRI B176 irregularity spectrum to closely represent the conditions [47]. The spatial wavelength range of the irregularity spectrum is set from 1 to 139 m, with a frequency count of 300, as shown in Fig. 10.

In the dynamic simulation, the track was configured as a straight section with the length of the track irregularity configured to 800 m. After the locomotive traverses the section with irregularities, it continues on a smooth track section. Accelerations were recorded at multiple measurement points on the bogie frame during the negotiation of the irregular track. The maximum value observed across these points is taken as the representative acceleration, as depicted in Fig. 10. Unless otherwise specified, all subsequent results presented are the maximum values obtained from the respective measurement points or wheelsets.

The dominant frequencies of acceleration depicted in Fig. 11, observed at four different speeds, align closely with the frequencies associated with hunting motion detailed in Table 3. Based on these observations, 3.5 Hz has been selected as the dominant frequency in case of unstable running behaviour, denoted as f_0, for use in the EN14363-based method.

The simulation speed was set to range from 60 to 400 km/h, and the lateral displacement of the wheelset on the smooth track was extracted as the outcome of the constant speed method. Additionally, the lateral force of the wheelset and the bogie frame acceleration

Table 3
Comparison of hunting motion frequency.

	HH	HL	MH	ML	LH	LL	JM3
Large-amplitude	3.7	3.2		3.5		3.3	3.3
Small-amplitude	9.3	8.8	7.7	7.9	6	5.3	

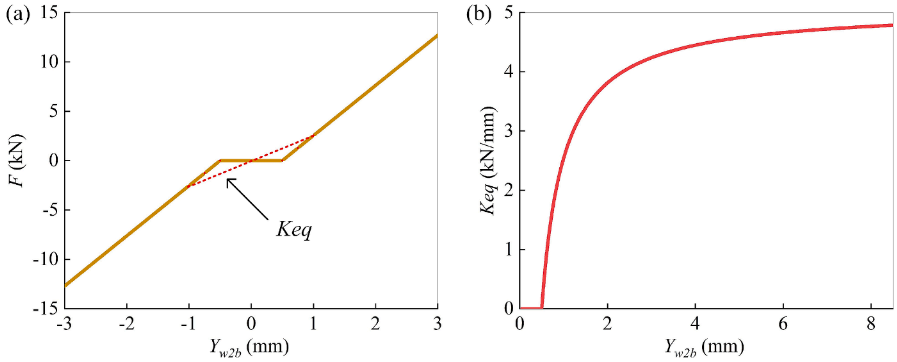

Fig. 8. Primary lateral stiffness linearization: (a) Force-displacement; (b) Equivalent stiffness-displacement.

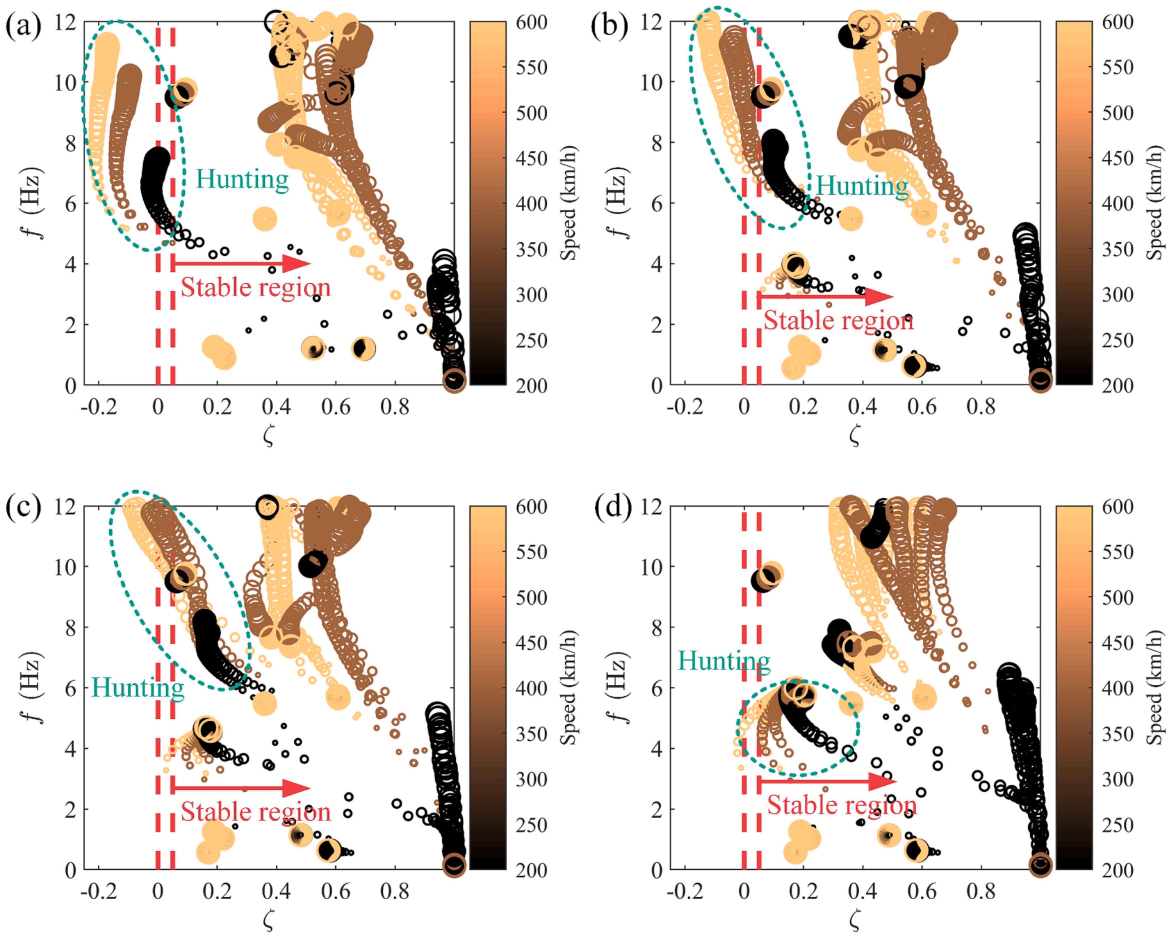

Fig. 9. Root loci of the locomotive model with variarion in conicity: (a) $Y_{w2b} = 0.5$ mm; (b) $Y_{w2b} = 0.75$ mm; (c) $Y_{w2b} = 1$ mm; (d) $Y_{w2b} = 8.5$ mm.

during operation on the irregular track were captured and processed according to the EN and GB standards. The results are illustrated in Fig. 12.

Fig. 12(a) illustrates a correlation between small-amplitude limit cycles and C_{s3} values, showing that higher C_{s3} values are linked to greater amplitudes of these limit cycles. Examination of Fig. 12(b) to (d) reveals that at lower velocities, the disparity between XL and XH is minimal. However, as the speed increases, locomotives with XH display significantly poorer stability in comparison to those with XL. Consequently, when subjected to the ERRI B176 track irregularity, the stability assessments based on the EN and GB standards are significantly influenced by the C_{g3} values. Specifically, an increased C_{g3} value is correlated with less favorable stability outcomes.

A compilation of critical speeds, derived from various stability assessment methods, is presented in Fig. 13. As shown in Fig. 13, the

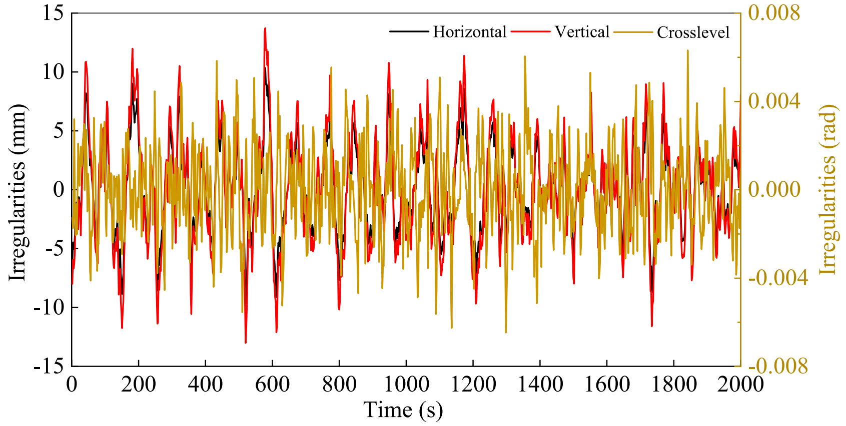

Fig. 10. Track irregulaities.

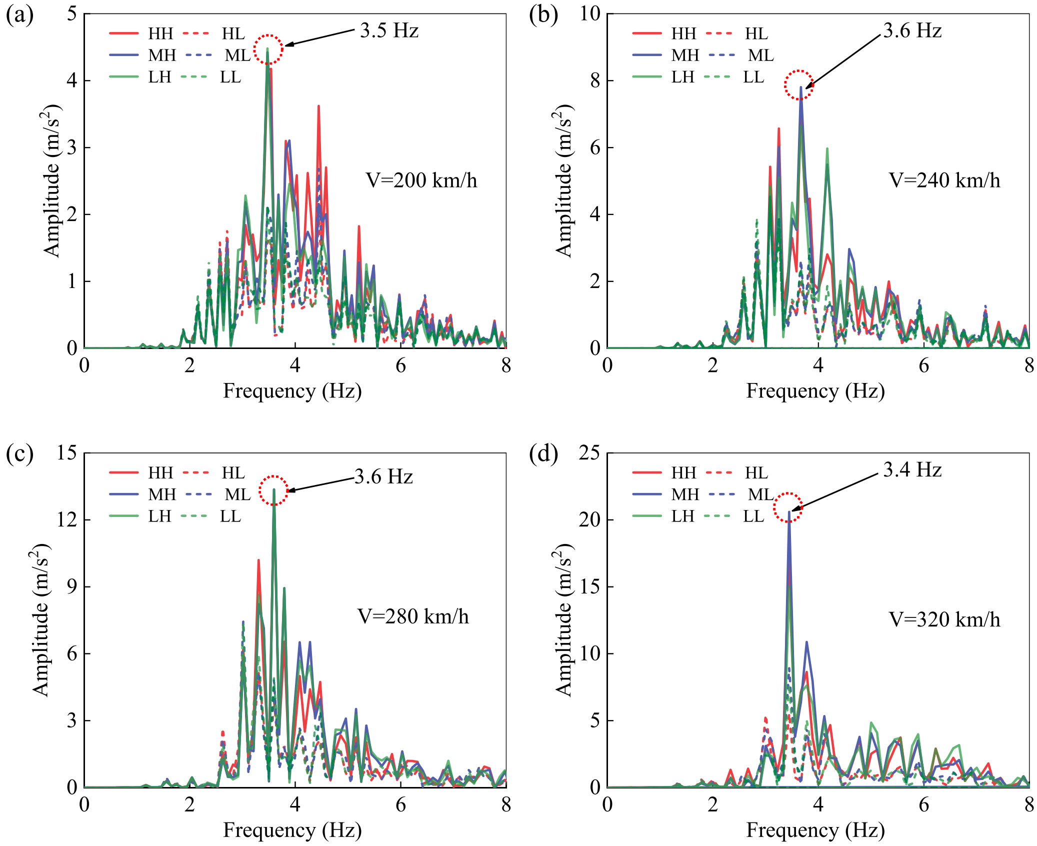

Fig. 11. Bogie frame acceleration.

Force EN, Acceleration EN, and Acceleration GB methods correspond to the determination of engineering critical speed. The constant speed method indicates the theoretical critical speed, while the decreasing method reflects the small-amplitude hunting critical speed.

Fig. 13 demonstrates a distinct pattern in the engineering critical speeds with ERRI B176 irregularity, exhibiting a negative correlation with the C_{g3} values. In contrast, the theoretical critical speeds display considerable variability, correlating negatively with the C_{s3} values. For conicity combinations HH and HL, the constant speed method leads to lower critical speeds than the Force EN, Acceleration EN, and Acceleration GB methods. Furthermore, all small-amplitude hunting critical speeds are observed to exceed 500 km/h, and this threshold is not significantly correlated with the characteristics of the equivalent conicity function.

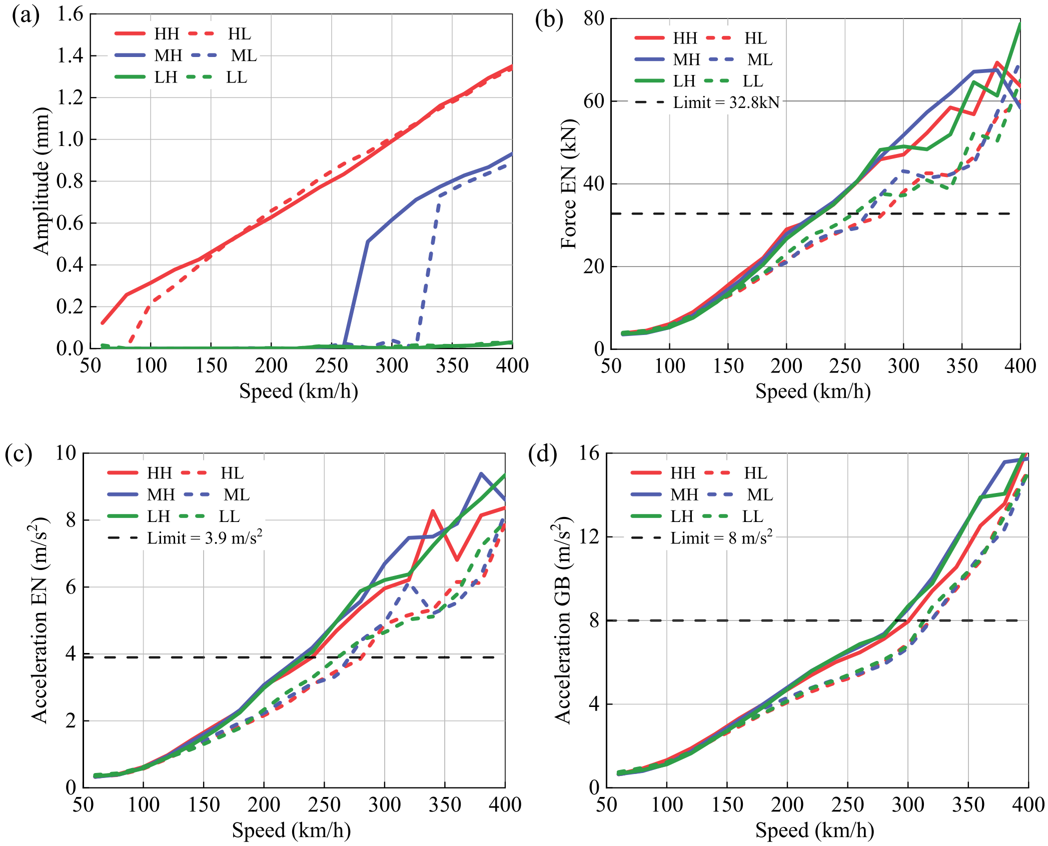

Fig. 12. Stability results considering track excitation: (a) Constant speed; (b) Force EN; (c) Acceleration EN; (d) Acceleration GB.

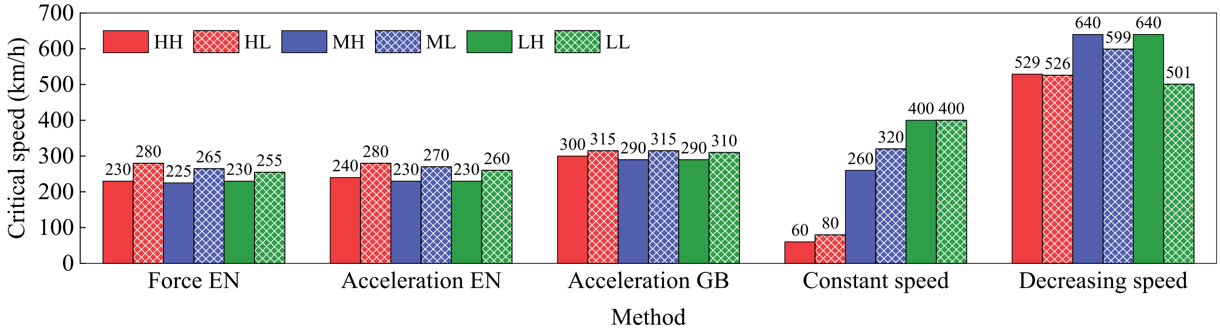

Fig. 13. Critical speed by different methods.

5.3. Stability evaluation based on DELR

Hunting motion significantly influences the dynamic performance of vehicles. The geometric contact matching between worn treads and the rail can result in a higher equivalent conicity, which in turn can cause increased lateral bogie vibration, termed secondary hunting. This phenomenon is more likely to occur at higher speeds. Conversely, when reprofiled treads match the rail, they create a lower equivalent conicity that may induce low-frequency car body oscillations, thereby affecting ride comfort. This phenomenon is referred to as primary hunting and typically occurs at lower speeds [45].

The increase in the amplitudes of both primary and secondary hunting results in an increase in the input energy involved in the vibration. We propose that the DELR evaluates stability by considering the energy input of hunting motion, thereby being applicable to both primary and secondary hunting. To substantiate this hypothesis, we employed thin flange profiles (JM3T) to simulate the conditions of primary hunting, characterized by low conicity. Subsequently, the six categories of worn flange profiles previously discussed were used to replicate secondary hunting, with the standard JM3 profile serving as a comparative baseline. The computational outcomes are depicted in Fig. 14.

Fig. 14 illustrates that the DELR increases monotonically with speed, without the fluctuations observed in Fig. 12. At lower speeds, locomotives with HX exhibit the poorest stability, whereas locpmotive with JM3T demonstrate a higher DELR compared to locomotive with JM3. Upon acceleration, locomotives matched with XH show the most pronounced decrease in stability. This finding emphasizes that DELR is capable of characterizing both primary and secondary hunting.

As mentioned earlier, hunting motion is a type of self-excited vibration, with its energy source being the kinetic energy from the vehicle's forward motion. The DELR metric is essentially related to the amount of energy input in the self-excited vibration. The main advantages of this metric include: firstly, it can adapt to various working environments and conditions, providing a unified evaluation standard for both high-frequency and low-frequency vibrations, which is why it can assess both primary and secondary hunting motions. Secondly, it reflects the continuous impact of vibrations over the entire time period, with vibrations of components such as wheels, motors, bogie frames, and the car body all influencing the DELR value. Lastly, DELR contributes to reducing energy consumption. Therefore, DELR can be considered a comprehensive evaluation metric.

In this study, no definitive threshold for DELR has been established to ascertain critical speeds, based on the insufficient breadth of experimental data and a desire to avoid premature or risky assessments. Nonetheless, DELR remains a valuable metric for evaluating stability and optimizing dynamic performance.

6. Summary and outlook

In this paper, we categorized equivalent conicity functions into six distinct classes and analyzed the stability of typical worn wheel treads using various assessment methods. Based on different stability evaluation criteria, several types of critical speeds have been proposed, namely the theoretical critical speed, small-amplitude hunting critical speed, and engineering critical speed. Furthermore, we developed the Driving Energy Loss Ratio (DELR), offering a novel metric for stability evaluation. The principal findings of this study include:

(1) The theoretical critical speed is greatly influenced by the equivalent conicity at small displacement, which can sometimes lead to overly conservative judgment results. Furthermore, the small-amplitude hunting critical speed poses a significant risk. Therefore, the engineering critical speed is recommended as a more reliable criterion for stability assessment and optimization.

(2) Using the decreasing method and root loci analysis on high-speed locomotives at higher speeds, it is observed that stability does not consistently worsen with an increase in conicity.

(3) Within the operational speed range of high-speed locomotives, the occurrence of small-amplitude hunting motion has a negligible influence on operational safety indicators. Employing the complete convergence of hunting amplitude to zero as the determinant of critical speed is deemed an excessively conservative criterion.

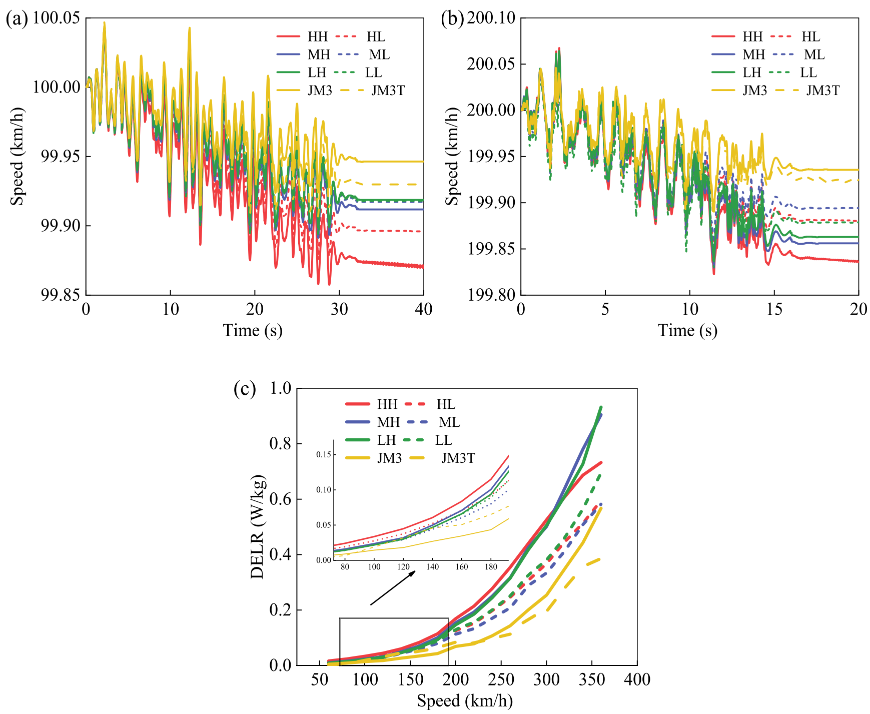

Fig. 14. Driving Energy Loss Ratio: (a) speed-time profile starting at 100 km/h; (b) speed-time profile starting at 200 km/h; (c) DELR with speed.

(4) The stability indicators in vehicle safety acceptance standards become increasingly sensitive to the equivalent conicity at lateral displacements exceeding 3 mm as velocity increases. Consequently, maintenance strategies for equivalent conicity should focus on values exceeding this threshold, instead of relying solely on the nominal equivalent conicity value.
(5) The DELR introduced in this study serves as an effective metric for assessing the stability of locomotives, demonstrating robust evaluative capabilities for hunting stability across a spectrum of high and low conicity conditions.

In locomotive design, it is often necessary to consider stability with worn wheel treads. This requires integrating multiple evaluation methods for design purposes. However, the conclusions of this study indicate that the theoretical critical speed is relatively conservative and should not be the primary guide for locomotive design. In fact, there is no absolute correlation between the three evaluation methods. For example, a high theoretical critical speed does not necessarily imply a high engineering critical speed.

The future directions outlined in this study encompass further investigation into the underlying causes of the patterns observed in second conclusion and the exploration of their applicability to diverse locomotive models and railway vehicles. The DELR metric introduced here is currently tailored to simulation scenarios, its adaptation for practical engineering applications would necessitate a holistic consideration of driving energy inputs, variations in gravitational potential energy, and the influence of additional resistive forces. DELR holds promise as an auxiliary index for stability optimization and assessment, yet it should not be relied upon as the exclusive criterion. To refine the threshold values of DELR, a broader spectrum of case studies must be integrated into the analysis.

CRediT authorship contribution statement

Hu Li: Writing – original draft, Validation, Software, Methodology, Formal analysis, Conceptualization. **Tong Tan:** Validation, Data curation. **Sebastian Stichel:** Writing – review & editing, Formal analysis. **Yuan Yao:** Supervision, Software, Funding acquisition.

Declaration of competing interest

The authors declare that they have no known competing financial interests or personal relationships that could have appeared to influence the work reported in this paper.

Acknowledgments

This work was supported by the National Natural Science Foundation of China [grant numbers 52372403, U2268211], the Sichuan Provincial Natural Science Foundation [grant number 2022NSFSC0034], and the National Railway Group Science and Technology Program [grant number N2023J071].

Data availability

Data will be made available on request.

References

[1] J.F. Sun, M.R. Chi, X.S. Jin, et al., Experimental and numerical study on carbody hunting of electric locomotive induced by low wheel-rail contact conicity, Veh. Syst. Dyn. 59 (2) (2021) 203–223.
[2] Y.X. Li, L.C. Dai, Z.T. Guo, et al., Carbody abnormal lateral vibration failure of high–speed train induced by the coupling factor of the wheel re-profiling method and excessive rail wear, Eng. Fail. Anal. 160 (2024) 108170.
[3] H.X. Gao, J.F. Sun, X.H. Chen, et al., A novel wheel wear indicator in regard to wheel-rail contact parameters and vehicle hunting stability, Eng. Fail. Anal. 167 (2025) 108967.
[4] Y.Y. Qi, H.Y. Dai, Y. Song, et al., Research on the characteristics of wheel hollow wear and suppression measures of high-speed trains, Tribol. Trans. 66 (4) (2023) 597–609.
[5] Y.B. Zhou, M.R. Chi, W.B. Cai, et al., Analysis of abnormal carbody lateral low-frequency vibration in intercity EMU trains caused by double-hollow worn wheel profiles, Eng. Fail. Anal. 167 (2025) 109065.
[6] J.Y. Guo, H.L. Shi, F.S. Li, et al., Field measurements of vibration on the car body-suspended equipment for high-speed rail vehicles, Shock Vib. (2020), https://doi.org/10.1155/2020/6041543.
[7] C. Chang, X. Ding, L. Ling, et al., Mechanism of high-speed train carbody shaking due to degradation of wheel-rail contact geometry, Int. J. Rail Transp. 11 (3) (2023) 289–316.
[8] J.A. Kaklar, R. Ghajar, H. Tavakkoli, Modelling of nonlinear hunting instability for a high-speed railway vehicle equipped by hollow worn wheels, Proc. Inst. Mech. Eng. Part K J. Multi-Body Dyn. 230 (4) (2016) 553–567.
[9] B. Nicola, M. Matteo, Z. Nicola, Simulation of wheel and rail profile wear: a review of numerical models, Railway. Eng. Sci. 30 (4) (2022) 403–436.
[10] B.G. Wen, S.H. Wang, G.Q. Tao, et al., Prediction of rail profile evolution on metro curved tracks: wear model and validation, Int. J. Rail Transp. 11 (6) (2023) 811–832.
[11] H.X. Li, L. Li, Z. Li, Research on the effect of rail cant on the dynamic performance and wear characteristics of subway vehicles, Eng. Fail. Anal. 152 (2023) 107478.
[12] Y.Y. Li, Z.S. Ren, R. Enblom, et al., Wheel wear prediction on a high-speed train in China, Veh. Syst. Dyn. 58 (12) (2020) 1839–1858.
[13] S. H-Nia, J. Flodin, C. Casanueva, et al., Predictive maintenance in railway systems: MBS-based wheel and rail life prediction exemplified for the Swedish Iron-Ore line, Veh. Syst. Dyn. 62 (1) (2024) 3–20.
[14] S. H-Nia, V.V. Krishna, K. Odolinski, et al., Simulation-based evaluation of maintenance strategies from a life cycle cost perspective, Wear 532 (2023) 205120.
[15] M.S. Sichani, R. Enblom, M. Berg, et al., A fast wheel–rail contact model for application to damage analysis in vehicle dynamics simulation, Wear 366 (2016) 123–130.
[16] R. Luo, B.B. Liu, S. Qu, A fast simulation algorithm for the wheel profile wear of high-speed trains considering stochastic parameters, Wear 480 (2021) 203942.

[17] I.S. Apezetxea, X. Perez, C. Casanueva, et al., New methodology for fast prediction of wheel wear evolution, Veh. Syst. Dyn. 55 (7) (2017) 1071–1097.
[18] I.S. Apezetxea, X. Perez, C. Casanueva, et al., Modelling stochastic excitations for a fast wear calculation methodology, Veh. Syst. Dyn. 58 (11) (2020) 1657–1674.
[19] S.S. Liu, Q.X. He, W.J. Fu, et al., A two-step data-driven method for predicting the wear of train wheel treads using GA-BPNN and LSTM algorithms, Int J Rail Transp. (2024), https://doi.org/10.1080/23248378.2024.2324092.
[20] S. Stichel, R. Persson, R. Giossi, Improving rail vehicle dynamic performance with active suspension, High-Speed Railw. 1 (1) (2023) 23–30.
[21] R. Giossi, R. Persson, S. Stichel, Wheel wear reduction of a mechatronic two-axle vehicle controlled with feedforward wheelset steering approaches, Veh. Syst. Dyn. 62 (4) (2024) 1037–1062.
[22] Y.G. Ye, J. Vuitton, Y. Sun, et al., Railway wheel profile fine-tuning system for profile recommendation, Railway. Eng. Sci. 29 (1) (2021) 74–93.
[23] K. Xu, Z. Feng, H. Wu, et al., Optimal profile design for rail grinding based on wheel–rail contact, stability, and wear development in high-speed electric multiple units, Proc. Inst. Mech. Eng. Part F-J. Rail Rapid Transit. 234 (6) (2020) 666–677.
[24] Y.G. Ye, Y.Y. Qi, D.C. Shi, et al., Rotary-scaling fine-tuning (RSFT) method for optimizing railway wheel profiles and its application to a locomotive, Railway. Eng. Sci. 28 (1) (2020) 160–183.
[25] Y.Y. Qi, H.Y. Dai, Y. Song, et al., Optimisation design of grinding rail profile of metro lines for small radius curved track based on the GFC method: a case study, Veh. Syst. Dyn. 62 (8) (2024) 1929–1951.
[26] U.I.C. Code, 518. Testing and approval of railway vehicles from the point of view of their dynamic behaviour-safety-track fatigue-ride quality, third ed., International Union of Railways, Paris, 2005.
[27] O. Polach, Characteristic parameters of nonlinear wheel/rail contact geometry, Veh. Syst. Dyn. 48 (sup1) (2010) 19–36.
[28] O. Polach, D. Nicklisch, Wheel/rail contact geometry parameters in regard to vehicle behaviour and their alteration with wear, Wear 366 (2016) 200–208.
[29] X.Q. Dong, Z.S. Ren, Z.Q. Xu, et al., Research on nonlinear characteristics and effect of equivalent conicity curve, J. Chin. Railway Soc. 40 (11) (2018) 91–97.
[30] Z.Q. Xu, X.Q. Dong, Research and verification on the nonlinear characteristics of wheel/rail equivalent conicity, in: Proceedings of the 26th Symposium of the International Association of Vehicle System Dynamics (IAVSD), 2020, pp. 678–685.
[31] R. Kulkarni, A. Qazizadeh, M. Berg, et al., Investigating the effect of the equivalent conicity function's nonlinearity on the dynamic behaviour of a rail vehicle under typical service conditions, Veh. Syst. Dyn. 60 (10) (2022) 3484–3503.
[32] K.K. Lyu, K.Y. Wang, P.F. Liu, et al., Analysis on the features and potential causes of wheel surface damage for heavy-haul locomotives, Eng. Fail. Anal. 109 (2020) 104292.
[33] P.F. Liu, K. Hao, C. Wang, et al., Investigation of curve minimum radius in heavy-haul railway to improve wheel wear evolution and wheel-rail contact geometry, Proc. Inst. Mech. Eng. Part F-J. Rail Rapid Transit. 238 (8) (2024) 895–906.
[34] J. Kalker, A fast algorithm for the simplified theory of rolling contact, Veh. Syst. Dyn. 11 (1982) 1–13.
[35] J.F. Sun, J.J. Gong, M.R. Chi, et al., Dynamic analysis of ultra-low frequency carbody swaying for a high-speed rail vehicle: Causes and measures, J. Vib. Control. (2024).
[36] Y.X. Li, M.R. Chi, Z.T. Guo, et al., An abnormal carbody swaying of intercity EMU train caused by low wheel–rail equivalent conicity and damping force unloading of yaw damper, Railway Eng. Sci. 31 (3) (2023) 252–268.
[37] J. Pombo, J. Ambrósio, M. Silva, A new wheel–rail contact model for railway dynamics, Veh. Syst. Dyn. 45 (2) (2007) 165–189.
[38] B.B. Liu, S. Bruni, Influence of individual wheel profiles on the assessment of running dynamics of a rail vehicle by numerical simulation: a case study, Veh. Syst. Dyn. 60 (7) (2022) 2393–2412.
[39] EN 14363:2016+A1- Railway applications - Testing and simulation for the acceptance of running characteristics of railway vehicles - Running behaviour and stationary tests, 2016.
[40] GB/T 5599-2019. Specification for dynamic performance assessment and testing verification of rolling stock. National Railway Administration, China, 2019.
[41] D. Skerman, C. Cole, M. Spiryagin, Determining the critical speed for hunting of three-piece freight bogies: practice versus simulation approaches, Veh. Syst. Dyn. 60 (10) (2022) 3314–3335.
[42] H. Li, Y. Yao, X.W. Chen, et al., Unstable limit cycle solution for hunting motion of railway vehicle based on initial state excitation method, China Railw. Sci. 39 (23) (2023) 78–83.
[43] H. Li, Y. Yao, X.W. Chen, Suspension parameter optimization for high-speed train with severe tread wear, Int. J. Rail Transp. (2024), https://doi.org/10.1080/23248378.2024.2345683.
[44] H. True, Multiple attractors and critical parameters and how to find them numerically: the right, the wrong and the gambling way, Veh. Syst. Dyn. 51 (3) (2013) 443–459.
[45] G. Li, R.D. Wu, X.X. Deng, et al., Suspension parameters matching of high-speed locomotive based on stability/comfort pareto optimization, Veh. Syst. Dyn. 60 (11) (2022) 3848–3867.
[46] Z.B. Zhang, P.B. Wu, R. Luo, et al., The relationship between contact angle difference and equivalent conicity of high-speed EMU, Adv. Mater. Res. 591–593 (2012) 1920–1924.
[47] X.M. Chen, L. Wang, X.X. Tao, et al., Study on general track spectrum for Chinese main railway lines, China Railw. Sci. 29 (3) (2008) 73–77.